



HAL
open science

Study of fast aeroelastic solvers for gust load computation

Oriol Chandre-Vila, Yann Nivet, Sylvie Marquier, Joseph Morlier, Nicolas Gourdain

► **To cite this version:**

Oriol Chandre-Vila, Yann Nivet, Sylvie Marquier, Joseph Morlier, Nicolas Gourdain. Study of fast aeroelastic solvers for gust load computation. International Forum on Aeroelasticity and Structural Dynamics IFASD 2022, Jun 2022, Madrid, Spain. 16 p. hal-03888181

HAL Id: hal-03888181

<https://hal.science/hal-03888181>

Submitted on 7 Dec 2022

HAL is a multi-disciplinary open access archive for the deposit and dissemination of scientific research documents, whether they are published or not. The documents may come from teaching and research institutions in France or abroad, or from public or private research centers.

L'archive ouverte pluridisciplinaire **HAL**, est destinée au dépôt et à la diffusion de documents scientifiques de niveau recherche, publiés ou non, émanant des établissements d'enseignement et de recherche français ou étrangers, des laboratoires publics ou privés.

STUDY OF FAST AEROELASTIC SOLVERS FOR GUST LOAD COMPUTATION

Oriol Chandre-Vila¹, Yann Nivet¹, Sylvie Marquier¹, Joseph Morlier², Nicolas Gourdain³

¹AIRBUS OPERATION SAS
316 Route de Bayonne, 31060 Toulouse, France
oriol.chandre-vila@airbus.com
yann.nivet@airbus.com
sylvie.marquier@airbus.com

²ICA, Universit de Toulouse, ISAE-SUPAERO, MINES ALBI, UPS, INSA, CNRS
3 Rue Caroline Aigle, 31400 Toulouse, France
joseph.morlier@isae-supero.fr

³ISAE-SUPAERO
10 Avenue Edouard Belin, 31055 Toulouse, France
nicolas.gourdain@isae-supero.fr

Keywords: Static Aeroelasticity, Fast Methodology, Unsteady Aerodynamics, Wind Gusts

Abstract: Aeroelasticity plays an important role in the design and certification of aircrafts. Whether steady aerodynamics is key for static methods, unsteady phenomenon is key for dynamic approaches. Nevertheless, in both aeroelastic problematics, it is basically aerodynamics who monopolizes the CPU cost. Thus, fast methods are interesting as alternative to the high cost of CFD/CSM simulations.

The aim of this study is to present an unsteady method that predicts the aerodynamics of aircrafts encountering a wind gust. First of all, the process that brought to the formulation of the static aeroelasticity from Wind Tunnel Tests (WTT) is refreshed [1]. It is a rapid and robust method based on the principle of the local incidence shift due to flexible effects. This difference in the angle of attack is used to interpolate the pressure coefficient from aerodynamics lookup tables.

Secondly, the static method (called *Fast Nonlinear Static Aeroelasticity* –FNSA–) is validated when analyzing a high aspect ratio wing which assures a flexible structure. The method deals with nonlinear, flexible and compressible effects in steady aerodynamics [2].

Finally, an algorithm is proposed to integrate the FNSA formulation to the unsteady problem of gust load computation. The methodology uses a quasi-steady approach of the static solver together with Wagner delay function modeling the unsteadiness of the flow [3]. Restricting our aeroelastic equation of motion to a simple mass-stiffness system, the airstream directed downward due to the gust is added to the downwash of each section. The formulation allows, then, a reaction to the gust at each time step that yields to flexible results with an accuracy comparable to the Unsteady Vortex Lattice Method but around 3600 times faster.

1 INTRODUCTION

The main goal of this paper is to present the chronological evolution of an unsteady methodology for load computation.

The original methodology used the concept of the effective angle of attack to correct low CPU cost methodologies and to introduce nonlinearities to the static aeroelastic solution [1]. The concept of computing an effective incidence that takes into account different contributions have been researched in the past years allowing to combine low CPU cost methodologies such as the Vortex Lattice Method (VLM) or the lifting line formulation with high-fidelity simulations [4]. This combination permits to correct the linear data with complex effects that are stored inside the rich simulations such as the compressibility effects, nonlinear behavior of the aerodynamics or the affectation of three-dimensionality to a particular section [5].

In addition, flexible effects can reduce the load on a section as they do not attempt to keep the original shape but to adapt the structural deformation. Yet, this behavior has effects on the wake development which, as consequence, makes aerodynamic lags play a relevant role on the dynamic response of the aircraft [6].

In the current situation of climate urgency where the unsteady phenomenon (i.e. clear-air turbulence or wind gusts) are expected to increase their presence in day-by-day operations for aircraft [7], together with the interest of slenderer and lighter wings, dealing with nonlinear flexible aeroelastic behavior is expected to be very beneficial.

Unsteady phenomenon has been studied from almost a century ago. Wagner concluded his experience of the response of a rigid airfoil with an analytical function for the aerodynamic delay due to arbitrary unsteady motion [8]. Theodorsen studied the problematic of a sinusoidal unsteady motion, notably modeling the effect of added mass to the lift and the pitching moment coefficient [9]. Küssner, on the other hand, proposed a delay function which pattern the response of a rigid airfoil to a gust [10]. And, finally, Jones assembled the three previous works and proposed the delays expressions for a finite wing [11].

In more recent years, alternatives to the well-known frequency domain Doublet Lattice Method (DLM) [12] are sought for the time domain. Such a milestone would make possible the unified computation of maneuver and gust loads [13]. It has been researched alternatives like combining panel methods to empiric delay functions [14], to complement a fast steady methodology with high-fidelity simulations for either filling a database that can be used to solve (in real time) any solution [15], or, correcting it with frequency and temporal approaches [16–18]. Another option studied is to create nonlinear reduced order techniques to gust computations [19].

However, one approach that has been largely investigated in different applications such as aircrafts or drones is the Unsteady Vortex Lattice Method (UVLM) [20]. In this approach, the linear circulation problem of the VLM is solved at each time step, adapting the terms to the effect of the wake to the panels of the wing and its own deformation.

Then, this work aims to present the time thread of the ongoing research of an unified methodology for maneuver and gust load computation. First of all, the wing tunnel tests (WTT) that are in the origin of the methods are remembered in Section 2 [1], presenting then the validation of the static method for nonlinear steady lift coefficient estimation for flexible wings in Section 3 [2]. Finally, the tool used to evolve the static method to the unsteady domain is presented and analyzed in Section 4 [3]. The latest focuses on the computation of gust loads as the unsteady test case.

2 ORIGIN OF THE CONCEPT

The basis of the method that it is being evolved emerged from the analysis of two different wind tunnel tests (WTT) results. Observing two rigid distinctive wing shapes (a common plan-form for both wings but one wing was representative of the cruise twist shape –named *1G*– and the second one had a twist shape representative of a high loaded maneuver flight point – named *2.5G*–), at each section it was possible to identify a constant difference of angle of attack between the two rigid shapes, as it is shown in Figure 1.

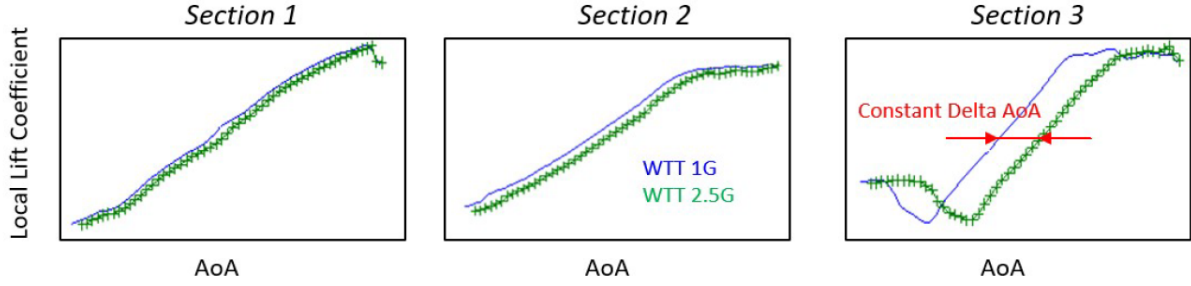


Figure 1: From the wing tunnel test (WTT) results, it is identified a constant $\Delta\alpha_{eff}$ between the local lift coefficient for two twist shapes in different wing sections [1].

Assuming that this discrepancy could be estimated in the linear zone, then be propagated to the full range of angle of attack and, assuming the 1G curve to be entirely known, the $\Delta\alpha$ applicable at each section can be computed using the following expression:

$$\Delta\alpha_{eff} \approx \frac{\Delta C_l}{\frac{\partial C_l}{\partial \alpha}} = \frac{AIC \cdot \Delta\theta}{AIC \cdot \{1\} \cdot \mathbf{n}_y} \quad (1)$$

where AIC calls for the Aerodynamic Influence Coefficient matrix (computed with a Vortex Lattice Method), $\frac{\partial C_l}{\partial \alpha}$ the lift slope of the 1G shape and $\Delta\theta$ the difference of twist between the two wing shapes. The lift gradient is computed using the AIC matrices and adapted to each section using the y-component of the normal vector \mathbf{n} .

Figures 2 and 3 exemplify this idea with a scheme: the effective angle of attack of any section can be computed by adding the geometrical angle of attack, the local twist and the angle induced by the other sections. Due to the forces experienced during the flight, the wing structurally deforms (which can be expressed as a difference in the twist $\Delta\theta$) and so it does the induced effect because it is basically a geometrical implication of a finite wing.

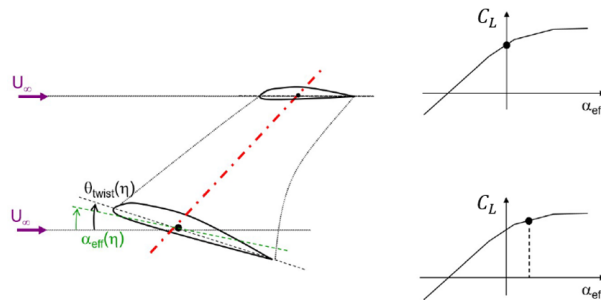


Figure 2: Local angles dissection for the initial wing configuration: the local effective total angle of attack is the sum of the geometric alpha, the twist and the induced angle: $\alpha_{eff}(\eta) = \alpha_{geo} + \theta(\eta) + \alpha_{ind}(\eta)$

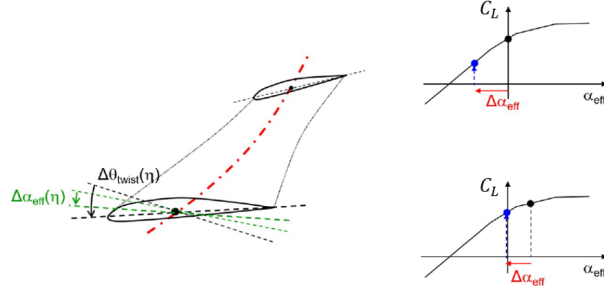


Figure 3: Local angles dissection for the deformed wing (or a second twisting law): $\Delta\alpha_{eff}(\eta) = \Delta\theta(\eta) + \Delta\alpha_{ind}(\eta)$

Then, this difference in effective angle of attack is used to update the local α for each spanwise section. Now, our local parameter has the nonlinear effects of the aeroelastic problem. Then, the full flexible aerodynamic performance can be reconstructed by considering the rigid behavior of a section at the incidence $[\alpha + \Delta\alpha_{eff}]$. This value can be used to interpolate the pressure coefficient from a database in order to correct our problem with high-fidelity data (i.e. RANS simulations, WTT or flight test data). Figure 4 schematizes the complete static aeroelastic loop.

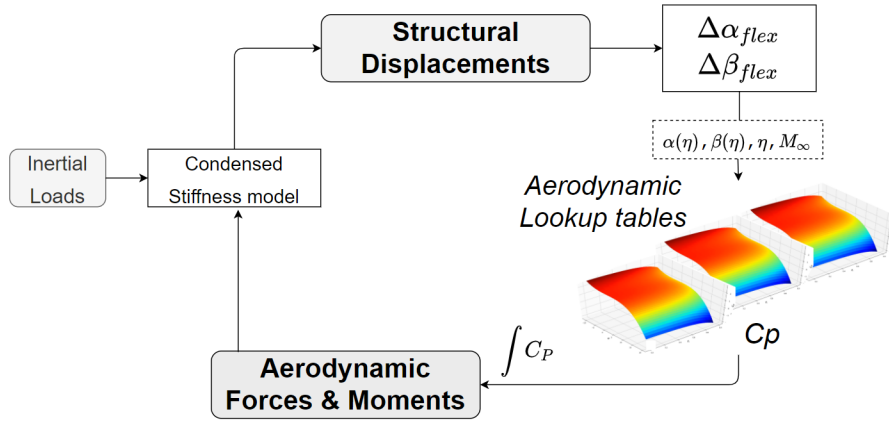


Figure 4: Static Aeroelastic Loop. Using a VLM method, the variation of α and β due to flexibility are computed from the structural displacements. Then, pressure coefficient C_p values are linearly interpolated from different lookup tables and integrated to compute aerodynamic forces and moments. Lookup tables can be filled with linear or nonlinear polars, WTT or flight test data.

The results presented in this work ambition to validate the aerodynamic model, thus the loop is not perform here. The *real* structural displacement is the input of our method and we compare the aerodynamic coefficients of the output to the *real* aerodynamic data. Figure 5 presents the performance of this flexible method against the WTT data, assuring accuracy for the whole range of incidences (which confirms the hypothesis).

Out of the scope of this work, the pitching moment coefficient was also tested giving great results [1]. In fact, if a similar mathematical approach was done from a moment point-of-view, another $\Delta\alpha$ would be derived. However, from a practical point of view, the formulation assures the accuracy, the speed and the robustness pretended for a load computation method.

After these results, no theoretical limits with respect to Mach regime (from low subsonic to high transonic) are expected since the local lift coefficient for all the sections along the wingspan could be deduced from one shape by applying a $\Delta\alpha_{eff}$. This is expected because considering

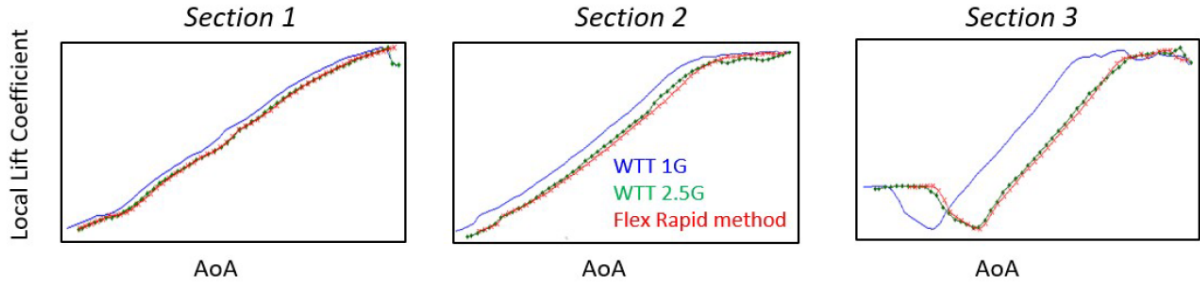


Figure 5: Local lift distribution, comparison with wind tunnel tests results [1].

the nonlinear onset driven by the same level of local lift for the both shapes is fully consistent with assumptions currently used in static aeroelasticity.

From now on, this flexible rapid solution is called *Fast Nonlinear Static Aeroelasticity* and it is identified with the acronym *FNSA*.

3 HIGH ASPECT RATIO FLEXIBLE WING RESULTS

The following step done in this ongoing research was to test the method at different Mach regimes (from low subsonic to high transonic) considering a flexible wing. XRF1 High Aspect Ratio Wing has been selected for that purpose. Figure 6 presents this wing which has an Aspect Ratio of $AR = 11.5$ and a flexible behavior ($\approx 10\%$ of tip displacement when flying at cruise regime [2]).

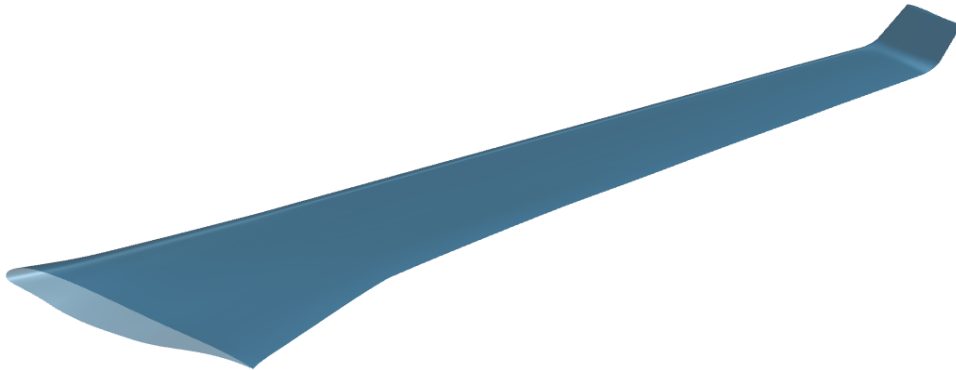


Figure 6: XRF1 High Aspect Ratio Wing with a winglet configuration.

The reader can see in Figure 7 the qualitative difference between the undeformed -blue- and deformed -red- shape. It is appreciated the interest of using the deformed shape to integrate the resultant aerodynamic forces and moments (feature that has been updated for this study).

This study has also been used to validate the compressible treatment proposed inside the methodology, which is basically adapting the x-coordinate position with the Prandt-Glauert correction [2] (with M_∞ the freestream Mach number):

$$\frac{x}{\sqrt{1 - M_\infty^2}} \quad (2)$$

In order to complement the formulation, an equivalence for the sideslip is proposed to Equation (1). This attribute is crucial for a future extension of the method to full aircraft in order to

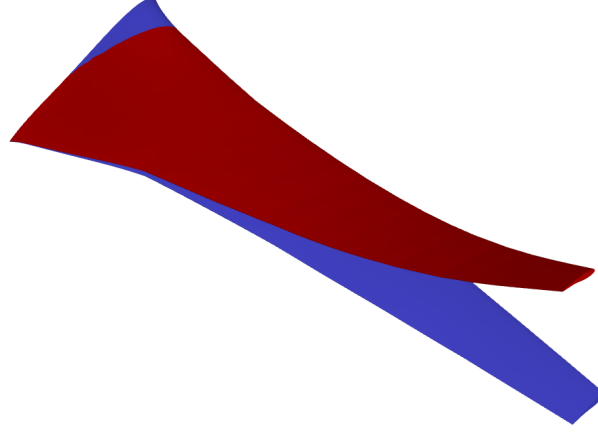


Figure 7: Nonlinear processing of the wing for the pressure coefficient C_p integration. Wing deformation due to fluid-structure interaction: in blue, the undeformed shape; in red, the deformed one.

take into account the Vertical Tail Plane (VTP), but also when considering a winglet configuration (like in this work). In such cases, the sideslip angle (β) can be seen as the directional angle of attack. Whether in α the twist is important, here it is the bending moment in the X-Y plane. Similarly, the gradient with respect to β is driven by the z-component of the local normal vector (\mathbf{n}_z):

$$\Delta\beta_{eff} = \frac{AIC \cdot \Delta\psi}{AIC \cdot \{1\} \cdot \mathbf{n}_z} \quad (3)$$

In Figure 8 the results of the proposed fast methodology (FNSEA) are compared against the high-fidelity aeroelastic simulations (Tau-CFD coupled with Nastran) [2]) for three different Mach regimes. In the first plot, we see that the method performs exactly the same as the reference solution. In the takeoff regime solution, we can visually appreciate a nonlinear behavior at high angle of attack (highlighting the nonlinear capabilities of the method). In this case, the error in lift coefficient is 3.8%. The third plot of the figure compares a cruise solution, giving an error of 4.7%. Even if they are not presented here, the use of the deformed shape to compute aerodynamic forces and moments improves the results of drag and pitching moment coefficient [2]. The errors appreciable in this plots may come from the aerodynamic mesh used for the RANS data stored in the lookup tables. With these results, the method is validated for capturing nonlinear flexible characteristics of the wing.

Being a pressure-based method, forces and moments are integrated from C_p , thus naturally the output are the pressure fields. In order to test this property, the C_p plots of different sections at a high-lift angle of attack is presented in Figure 9. The error committed in this regime is of $\approx 8\%$, which confirms the implementation of the method at all Mach regimes.

4 AN UNSTEADY FRAME FOR THE STATIC SOLVER

After the static aeroelasticity study, our ambition is to continue exploring the limits of this method in an unsteady problem. With this ambition, an algorithm is proposed in order to estimate the lift force considering the unsteadiness of the flow. Gust loads are regulated and a $1 - \cosine$ model is proposed to shape the vertical disturbance [21]:

$$\frac{w_G(t)}{U_\infty} = \frac{GR}{2} \cdot \left[1 - \cos\left(2\pi \frac{U_\infty \cdot t}{H}\right) \right] \quad (4)$$

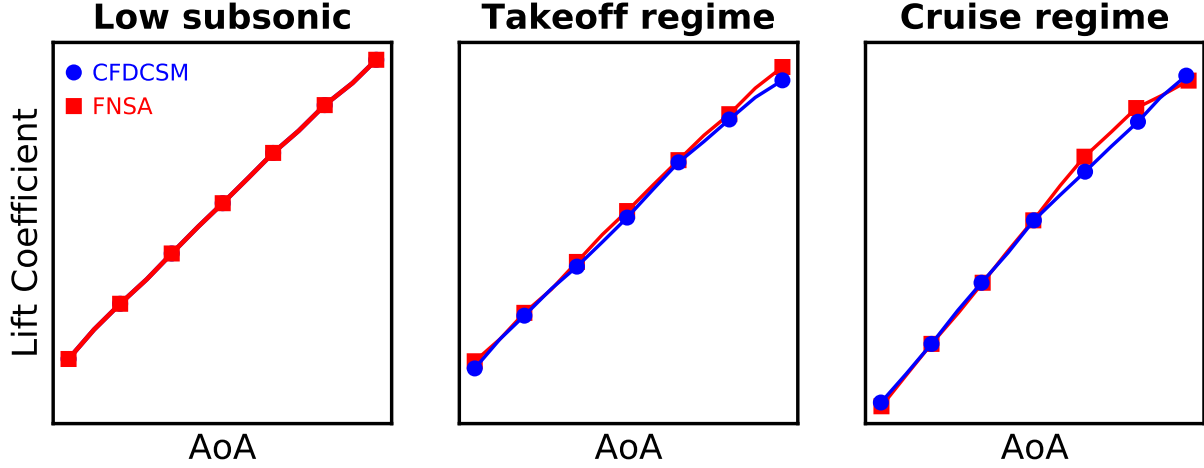


Figure 8: FNSA lift coefficient validation against high-fidelity CFDCSM result for different Mach regimes.

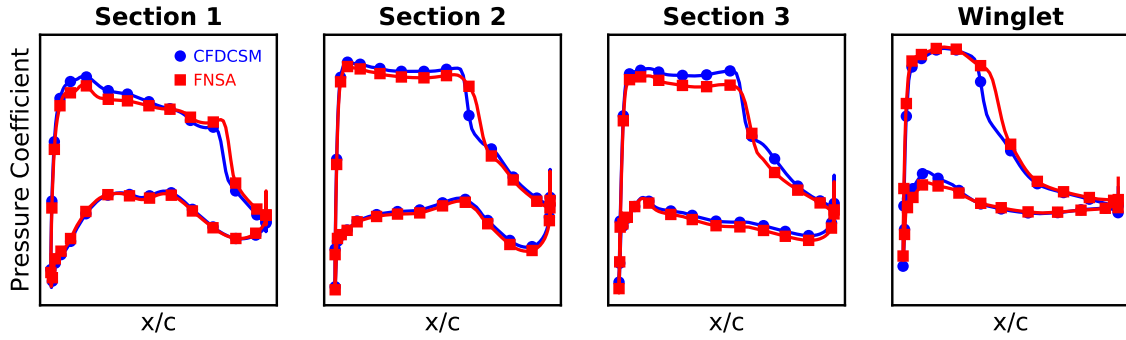


Figure 9: FNSA local pressure coefficient validation against high-fidelity CFDCSM result for cruise regime and high lift angle of attack.

where U_∞ is the freestream speed, H the gust length and GR the *Gust Ratio* which parametrizes the intensity of gust.

So, the impact of the gust to aerodynamic forces depends on the values of GR and H . The first parameter is easy to evaluate: the highest the amplitude of the gust, the highest the load; with no effect of delay. However, evaluating the impact of the gust length is more complex because it defines the unsteady character of the flow. From regulations [21], gust lengths must be checked from 9 m to 107 m. These gusts lengths can be converted to reduced frequency (dimensionless) using [22] in order to classify how unsteady is our problem:

$$k = \frac{\omega \cdot b}{U_\infty} \quad (5)$$

where b is the semi-chord and, ω the circular frequency $\omega = 2\pi \cdot f$, which value depends on the gust length (H), as expressed by Equation 6.

$$f = \frac{U_\infty}{2 \cdot H} \quad (6)$$

The final expression of k is defined in Equation 7 and, in Table 1, the values of the frequency and its degree of unsteadiness are identified.

$$k = \frac{\pi \cdot c}{2 \cdot H} \quad (7)$$

Table 1: Unsteady classification of gusts defined using Equation 4. Reduced frequency k (dimensionless) is defined using Equation 7.

H , m	k	Unsteady classification
9	0.31	Highly unsteady
58	0.05	Unsteady
107	0.03	Quasi-steady

From previous research, the shortest the gust the highest the unsteadiness degree of the problem. Besides, the lag between a quasi-steady and unsteady loads varies with respect to k [22, 23]. Figure 10 presents the gust profile for the three different reduced frequency studied in this work.

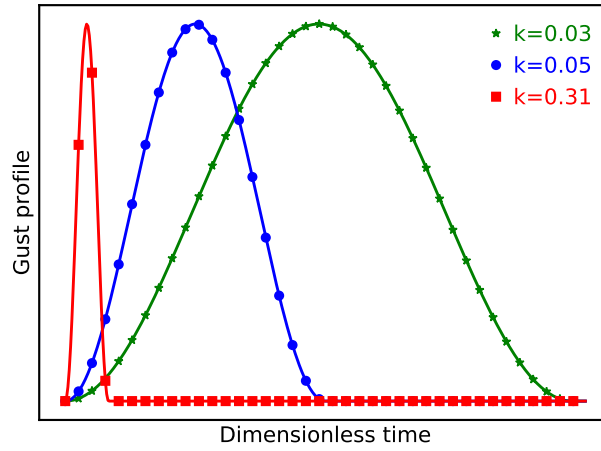


Figure 10: Gust profiles for different reduced frequency k when flying at a takeoff regime and $\alpha = 0^\circ$ encountering a gust of intensity $GR = 0.5$.

The wing used for this study is the academic rectangular wing, named *Goland wing* for aerosturctural purpose [24]. In Table 2, the characteristics of the wing are presented and Figure 11 shows the wing-box structure of the full wing which has the first mode (bending) at 1.93 Hz and the second mode (torsion) at 3.94 Hz .

Table 2: Characteristics of the Goland Wing.

Planform	Rectangular
Profile	Flat plate
Chord, m	1.8
Wingspan, m	12
Aspect Ratio	6.7
f_h , Hz	1.93
f_α , Hz	3.94

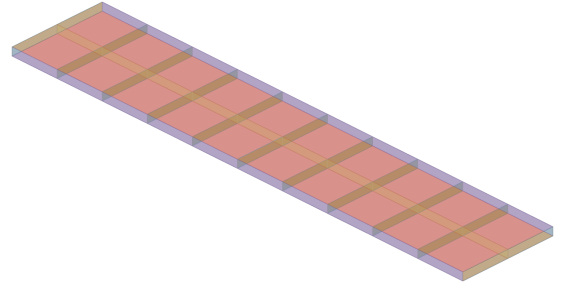


Figure 11: Wing-box structure of the Goland Wing.

The aeroelastic equation of motion (EOM) that is solved in this first approach to unsteady problems is a mass-stiffness system:

$$\begin{bmatrix} m_w & S_w \\ S_w & I_w \end{bmatrix} \cdot \begin{bmatrix} \ddot{h}(t) \\ \ddot{\alpha}(t) \end{bmatrix} + \begin{bmatrix} k_h & 0 \\ 0 & k_\alpha \end{bmatrix} \cdot \begin{bmatrix} h(t) \\ \alpha(t) \end{bmatrix} = \begin{bmatrix} L(t) \\ M_y(t) \end{bmatrix} \quad (8)$$

where m_w is the mass of the wing (6600 kg), S_w is the static imbalance around the pitching axis, I_w is the moment of inertia around the pitching axis, k_h and k_α are the stiffnesses of the springs providing restoring loads in the plunge and pitch degrees of freedom, respectively, and L and M_y are the lift and moment around the pitching axis. The terms of the mass and stiffness matrix are computed as:

$$\begin{cases} S_w &= -m_w x_{ea} \\ I_w &= \frac{m_w c_0^2}{12} + m_w c_0^2 x_{ea}^2 \\ k_h &= m_w (2\pi f_h)^2 \\ k_\alpha &= I_w (2\pi f_\alpha)^2 \end{cases} \quad (9)$$

with c_0 the root chord and, x_{ea} the elastic axis position. The direction of the axis and the distances are defined using Theodorsen's typical section, which is presented in Figure 12. The elastic axis is defined at the leading edge of the root chord (i.e. $x_{ea} = -b$).

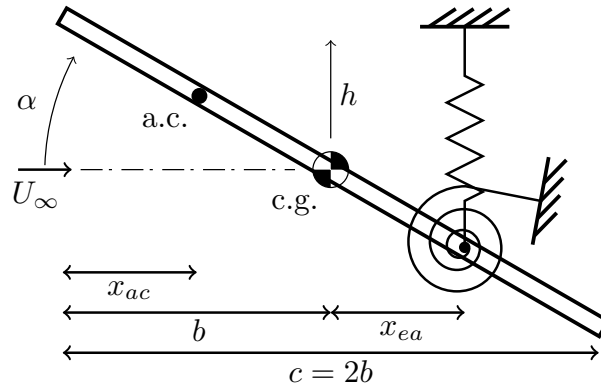


Figure 12: Theodorsen typical section model.

Different requirements need to be satisfied by the chosen unsteady frame in order to handle our formulation. First of all, the quantity of unsteady high-fidelity simulations should be the lowest possible (ideally, no unsteady simulations to be run). This requirement prevent us to use these simulations to be the ending condition of our iteration [17].

Secondly, the formulation should stand for a pressure-based methodology since FNSA interpolates the C_p and all the interest quantities are computed afterwards. This requirement is an advantage because flexible and compressible effects will be added thanks to the static formulation, as it has been demonstrated in the previous sections.

The fastest solution would be to use empiric functions that model the delay and the impact of unsteady aerodynamics to the load [8, 10]. Published methodologies uses the Wagner function to correct a quasi-steady fast lifting line solver, which yields to 3D unsteady solutions. In the work, the Wagner Lifting Line (WLL) is evaluated for the calculation of unsteady motion lift forces giving low CPU costs [14].

Such formulation it is really interesting because it defines the circulatory lift by means of the integral of pressure coefficient along the wingspan:

$$C_L^c(t) = \int \delta C_P(y) dy \quad (10)$$

But it can also be computed by performing the convolution of the downwash of each section w and a delay function. Since the circulatory lift is the force due to the motion [25], this delay

function is the one proposed by Wagner ϕ :

$$C_L^c(t) = a_0 \left(\frac{w(t)}{U_\infty} * \phi(t) \right) \quad (11)$$

where a_0 is the lift slope and, w is the sum of the downwash originated due to the local incidence, due to the plunge rate, due to the rotation rate and due to three dimension effects:

$$w(t) = U_\infty \cdot \alpha(t) + \dot{h}(t) + \dot{\alpha}(t) \cdot d + w_{3D}(t) \quad (12)$$

In order to introduce the convolution definition in a system of equation, Equations 10 and 11 are reformulated using what the authors call *aerodynamic states* in order to integrate the convolution concept as a new entry of the system. Then, bringing also Equation 8 to the system, a linear differential equation is defined:

$$A\dot{y} = By + C \quad (13)$$

where matrices A , B and C can be defined following the methodology described in [14] and array of unknowns y contains the time varying Fourier coefficients, the aerodynamic states and the two DOF (h and α).

Going deeper with the lift term, the classical unsteady formulation considers two contributions: circulatory lift and non-circulatory effect. This term (also known as the added mass term) expresses the inertia of the fluid derived from the fact that the flow and the airfoil cannot exist at the same place at the same moment. The lift and the moment of non-circulatory contributions where derived by Theodorsen [9]:

$$C_L^i(t) = \frac{a_0 \cdot b}{2 \cdot U_\infty^2} \left\{ \ddot{h}(t) + a \cdot b \cdot \ddot{\alpha}(t) \right\} - \frac{a_0 \cdot b}{2 \cdot U_\infty} \dot{\alpha}(t) \quad (14)$$

$$C_M^i(t) = -\frac{a_0 \cdot b}{4 \cdot U_\infty^2} \left\{ (a \cdot \ddot{h}(t) + b \cdot \left(a^2 + \frac{1}{8} \right) \cdot \ddot{\alpha}(t)) \right\} + \frac{a_0 \cdot b}{4 \cdot U_\infty} \cdot \left(a - \frac{1}{2} \right) \dot{\alpha}(t) \quad (15)$$

where a is the dimensionless position of the elastic axis.

When a body encounters a gust, typically a new term to C_L is added to sum-up the new contribution:

$$C_L = C_L^i + C_L^c + \Delta C_L^G \quad (16)$$

and, since C_L^c and ΔC_L^G applied to the aerodynamic center, the pitching moment term is:

$$C_M = C_M^i + \left(\frac{1}{4} + \frac{a}{2} \right) \left(C_L^c + \Delta C_L^G \right) \quad (17)$$

The term that expresses how much lift is created due to the gust is defined as:

$$\Delta C_L^G(t) = a_0 \left(\frac{w_G(t)}{U_\infty} * \psi(t) \right) \quad (18)$$

where ψ is the Küssner delay function.

However, the mass-stiffness problem of just 2 DOF limits the flexible capacity of our approach because we are using rigid-nature delay functions without adding more representative modes to

our problem. Thus, in order to overpass this limitation, the ΔC_L^G term is not computed and the gust downwash is introduced to the expression of w :

$$w(t) = U_\infty \cdot \alpha(t) + \dot{h}(t) + \dot{\alpha}(t) \cdot d + w_{3D}(t) + w_G(t) \quad (19)$$

This is supported from a physical point of view: the wing do not differentiate whether the air is moving because of a gust or because it is actually moving. With this modification, it is expected the solver to adapt to gust at each time step, yielding to flexible loads [3].

Figure 13 presents the performance of the two options: in blue when $C_L = C_L^i + C_L^c + \Delta C_L^G$ and in red when $C_L = C_L^i + C_L^c(w_G)$. The undelayed solution is also plotted here for a quasi-steady gust of $GR = 0.5$ and $k = 0.03$. The load alleviation between the blue and the red plot can be identified as the difference between flexible and rigid loads [26]. Thus, the approach of Equation 19 is able to introduce the flexible behavior of the wing even if solving a restrictive aeroelastic EOM.

The undelayed solution is computed using the same approach as the blue plot but without the delay functions. Thus, the green curve is the result of gust downwash unfiltered (i.e., without modeling the transition that Aerodynamics needs to achieve the steady-state value).

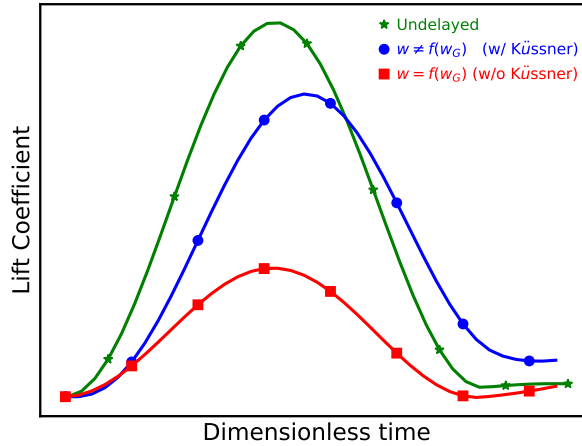


Figure 13: Comparison of the different methodologies when the Goland wing flying at a takeoff regime and $\alpha = 0^\circ$ encounters a gust of reduced frequency $k = 0.03$ and intensity $GR = 0.5$. In green, the result of gust downwash unfiltered, in blue when $C_L = C_L^i + C_L^c + \Delta C_L^G$ and, in red, when $C_L = C_L^i + C_L^c(w_G)$.

After this analysis, the retained methodology is the one that incorporates the gust within the downwash expression. Then, Equation 10 can be computed using a quasi-steady approach of FNSA and the value can be corrected using Equation 11.

Algorithm 1 details the steps proposed to converged the unsteady solutions using the static methodology (called *uFNSA*). As inputs, the solver needs the initial conditions of the two DOF. Normally, h_0 , $\ddot{\alpha}_0$ and \dot{h}_0 are zero, but α_0 cannot be. It is also need the final value of time and the desired time step. In order to define Δt , the Nyquist-Shannon theorem is used knowing that for the longest gust the limiting frequency is the bending eigenfrequency, but for the shortest it is the gust eigenfrequency. In order to accelerate the solver, w_{3D} is precomputed for several Mach regimes and angle of attacks and it is interpolated at step 9. If in the Wagner Lifting Line process the 3D effects are computed using the lifting line approach, here a Vortex Lattice Method (VLM) is used for that purpose. Since the time varying Fourier coefficients are not computed because the lifting line is no longer used, the array of unknowns is smaller and the same applies for the size of the matrices.

Algorithm 1 Algorithm for uFNSA computation.**Input:** q_0, \ddot{q}_0 (initial conditions), t_{end} and Δt **Output:** $C_L(t)$ (time-story of lift coefficient)

```

1: procedure uFNSA( $q_0, \ddot{q}_0, t_{end}, \Delta t$ )
2:    $C_L[0] \leftarrow$  FNSA( $q_0, \ddot{q}_0$ ) ▷  $C_L$  for  $t = 0$ 
3:    $t_i \leftarrow 0$ 
4:   while  $t_i \neq t_{end}$  do
5:      $C_{Lold} \leftarrow C_L[t_i]$  ▷ Recovering old value
6:      $t_i \leftarrow t_i + \Delta t$  ▷ Advancing in time
7:     while  $\varepsilon > 10^{-5}$  do
8:        $w_G \leftarrow$  gust( $t_i$ ) ▷ Equation 4
9:        $w_{3D} \leftarrow$  VLM( $q$ )
10:       $w \leftarrow$  downwash( $q, w_G, w_{3D}$ ) ▷ Equation 19
11:       $C_L^c, C_M^c \leftarrow$  circLift( $w$ ) ▷ Equation 11
12:       $C_L^i \leftarrow$  noncircLift( $q, \ddot{q}$ ) ▷ Equation 14
13:       $C_M^i \leftarrow$  noncircMomt( $q, \ddot{q}$ ) ▷ Equation 15
14:       $q, \ddot{q} \leftarrow$  EOM( $C_L^c, C_M^c, C_L^i, C_M^i$ ) ▷ Equation 8
15:       $C_{Lnew} \leftarrow$  FNSA( $q, \ddot{q}$ )
16:       $\varepsilon \leftarrow$  abs( $C_{Lnew} - C_{Lold}$ )
17:    end while
18:     $C_L[t_i] \leftarrow C_{Lnew}$  ▷ Filling the time-story
19:  end while
20:  return  $C_L(t)$ 
21: end procedure

```

A notable difference between FNSA and WLL methodologies is the treatment of the pitch DOF that results of Equation 8. FNSA understands that the value resulting from the aeroelastic linear EDO system is in fact the torsion θ and it is converted to the aerodynamic α using Equation 1. However, the lifting line method uses the EOM value directly as an aerodynamic parameter.

In order to validate the formulation, the Unsteady Vortex Lattice Method (UVLM) is used [20]. It is a potential solution for the continuity equation in the time-domain:

$$AIC \cdot \Gamma(t) = b(t) \quad (20)$$

AIC matrix only depends on the geometry of the wing. So, for low flexibility aircrafts, unsteadiness is introduced just by the RHS term. This term is actualized at each time step when the line of vortex at the trailing edge leaves the wing to join the wake geometry, moving all the others wake vortex one step away from the wing. When considering the gust, the RHS at random panel p yields to Equation 21, with Q_∞ the freestream speed 3D-vector and \mathbf{n}_p the normal to the panel.

$$b_p(t) = -(Q_\infty + w_{3D}(t) + w_G(t))_p \cdot \mathbf{n}_p \quad (21)$$

However, this equation does not just take into account the gust effects on the bound vortex. After surpassing the wing, the gust affects the wake vortex by modifying its position. In this approach, the induced velocity w_{3D} seen by the wing will adapt due to the gust at each iteration. In order to assess the suitability of UVLM for these cases, the experimental wake patterns for a profile validated the model up to $k = 8.5$ with parallel streamlines to trailing edge until $k = 0.6$,

which does not affect the lift and pressure coefficient C_p in a visible manner [20]. Furthermore, the vertical kinematic velocity of the trailing edge was found to play an important role, with a proposed limitation of this displacement at $\frac{h}{U_\infty} \ll 1$, verified for our problem [20]. Finally, when verifying the suitability to finite wings, no exclusive information has been found. Only on a work that challenges the hysteresis lift beyond $k = 0.15$ at $M_\infty = 0.29$ regime [17]. Thus, it is selected as the reference solution because it solves the continuity equation at each time step while considering the effect of the wake into the wing.

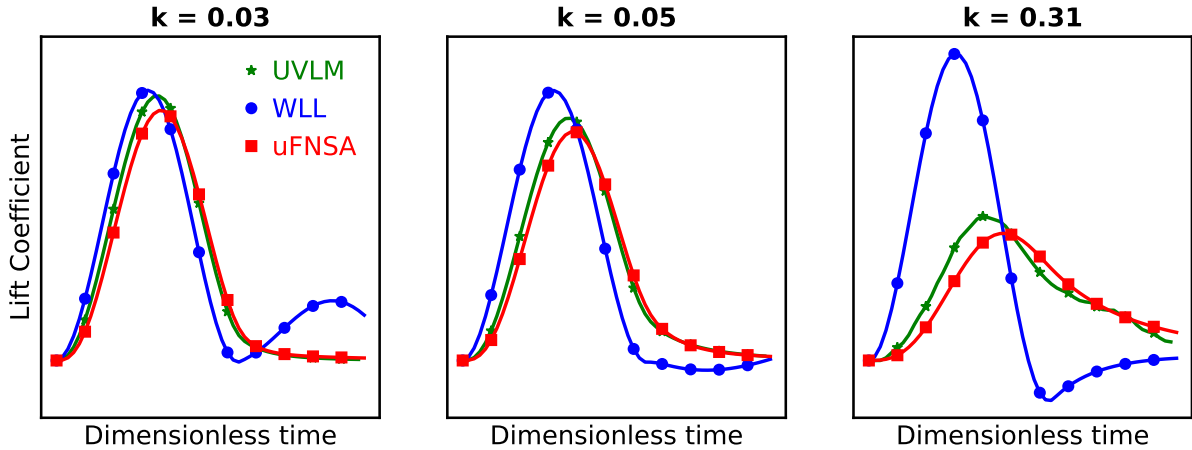


Figure 14: Comparison of the lift coefficient at different reduced frequency k when flying at a takeoff regime and $\alpha_0 = 0^\circ$ encountering a gust of intensity $GR = 0.5$. Unsteady FNSA is compared to Unsteady Vortex Lattice Method (UVLM) and Wagner Lifting Line (WLL) applied to gusts.

Figure 14 presents the results of the Golland wing flying at a takeoff-type regime, encountering a vertical gust of the $GR = 0.5$. Even if uFNSA formulation can deal with all kind of data (from linear polars to flight test data), in this work the aerodynamic lookup tables are filled with C_p computed using a VLM approach in order to properly compared to the linear solutions.

When the longest gust ($k = 0.03$) is evaluated, both methods are accurately predicting the load peak value and the time in which it happens: the load value error is of 2% for WLL and 5% for uFNSA whereas the lag errors are 10% and $< 1\%$, respectively. This was expected because of the quasi-steady formulation of both strategies. However, when the wing enters a purely unsteady domain ($k = 0.05$), WLL starts to misperform (11% for the load and 15% for the lag). On the contrary, uFNSA responded exactly the same way as it did in the previous case. Finally, when trying a short gust ($k = 0.31$), WLL completely mismatches UVLM, which is not unexpected because of the limitations from its formulation. And, uFNSA commits assumable errors of 11% error for the load and 20% for the lag. These errors could be explained using the low values (absolute differences are 0.05 lift units and 0.001 seconds). Nevertheless, these errors could be also explained by the use of steady data to compute highly unsteady loads.

Thus, WLL was a first attempt that gave accurate results until the limit of quasi-steadiness, and using the information stored within a database, uFNSA reproduced UVLM solutions for all cases.

5 CONCLUSION

After highlighting the advantages of the previous presented static solver [1], the method has been tested in a high flexible wing giving accurate results in a typical range Mach regimes of a commercial aircraft.

Furthermore, we started the second part of this work aiming a method that could easily adapt to a changing environment because we need to assess how wind gusts impact the loads on our wing. Because of that, we used intensity of gusts that are not related to the gust length (as it is for EASA CS-25 regulation [21]).

And it has been tested that combining steady data with unsteady strategies provides these accurate results that would allow the assessment of the impact of gusts in a any aircraft. In addition, the formulation introduced relies on different types of data.

Another requirement was to develop a fast and, above all, robust solver. With the static aeroelastic solver well integrated into unsteady frame, the gust load computation is solved in less than one second. The strategy gives the same results as the Unsteady Vortex Lattice Method around 3600 times faster (CPU time for UVLM is of the order of magnitude of hours). Finally, with the database filled, it will always return a solution. So the robustness of the method is also assured.

Finally, it is though that introducing the gust into the downwash empowers Physics to adapt, giving space to the evaluation of flexible effects more naturally. It is also expected a nonlinear behavior when using high-fidelity data. However, these nonlinearities will be related to a static problem, which can be a limitation to the unsteady load overshoot.

6 WAY FORWARD

Thus, an improvement is needed if this overshoot wants to be assessed. That could probably be done correcting the method in a similar way as it is done with Doublet Lattice Method [16, 27].

Following the present study, it is ambioned to test the new unsteady formulation in a more representative wing such as th XRF1 HARW with higher aspect ratio and more flexible. In other words, to a wing closer to the commercial one.

Finally, it would be also interesting to introduce a measure of the certainty of the solution. For instance, a result of a problem of $k = 0.05$ the value would be much smaller a highly unsteady problem. That could help users identifying the need of a possible fully unsteady high-fidelity aeroelastic simulation.

7 REFERENCES

- [1] Barriety, B., Boin, J.-P., Chandre-Vila, O., et al. (2019). Fast fluid-structure computational method taking into account non-linear aerodynamic. In *18th International Forum on Aeroelasticity and Structural Dynamics*.
- [2] Chandre-Vila, O., Boin, J.-P., Barriety, B., et al. Fast nonlinear method for static aeroelasticity applied to high aspect ratio wings at different mach regimes. *Under review*.
- [3] Chandre-Vila, O., Nivet, Y., Morlier, J., et al. (2020). Fast methods for dynamic fluid-structure interactions considering unsteady aerodynamic. In *AIAA SCITECH 2022 Forum*. doi:10.2514/6.2022-2538.
- [4] van Dam, C. P. (2002). The aerodynamic design of multi-element high-lift systems for transport airplanes. *Progress in Aerospace Sciences*, 38(2), 101–144. doi:10.1016/S0376-0421(02)00002-7.

- [5] Parenteau, M., Sermeus, K., and Laurendeau, E. (2018). Vlm coupled with 2.5d rans sectional data for high-lift design. In *2018 AIAA Aerospace Sciences Meeting*. doi: 10.2514/6.2018-1049.
- [6] Murua, J., Palacios, R., and Graham, J. M. R. (2012). Assessment of wake-tail interference effects on the dynamics of flexible aircraft. *AIAA Journal*, 50(7), 1575–1585. doi:10.2514/1.J051543.
- [7] Cheng, C. S., Lopes, E., Fu, C., et al. (2014). Possible impacts of climate change on wind gusts under downscaled future climate conditions: Updated for canada. *Journal of Climate*, 27(3), 1255–1270.
- [8] Wagner, H. (1925). Über die entstehung des dynamischen auftriebes von tragflügeln. *ZAMM Journal of Applied Mathematics and Mechanics*, 5(1), 17–35. doi: 10.1002/zamm.19250050103.
- [9] Theodorsen, T. (1935). Theory of aerodynamic instability and the mechanism of flutter. Tech. rep., NACA Library.
- [10] Kussner, H. G. (1936). Zusammenfassender bericht ber den instationren auftrieb von flügeln. *Luftfahrtforschung*, 13(12), 410–424.
- [11] Jones, R. T. (1940). The unsteady lift of a wing of finite aspect ratio. Tech. rep., NACA Library.
- [12] Rodden, W. P., Giesing, J. P., and Kalman, T. P. (1972). Refinement of the nonplanar aspects of the subsonic doublet-lattice lifting surface method. *Journal of Aircraft*, 9(1), 69–73. doi:10.2514/3.44322.
- [13] Kier, T. (2018). An integrated modelling approach for flight dynamics, manoeuvre- and gust-loads analysis. In *AIAA SCITECH 2018 Forum*. doi:10.2514/6.2018-2209.
- [14] Boutet, J. and Dimitriadis, G. (2018). Unsteady lifting line theory using the wagner function for the aerodynamic and aeroelastic modeling of 3d wings. *Aerospace*, 5, 92. doi: 10.3390/aerospace5030092.
- [15] Skujins, T. and Cesnik, C. E. S. (2014). Reduced-order modeling of unsteady aerodynamics across multiple mach regimes. *Journal of Aircraft*, 51(6), 1681–1704. doi: 10.2514/1.C032222.
- [16] Kier, T., Verveld, M., and Burkett, C. (2015). Integrated flexible dynamic loads models based on aerodynamic influence coefficients of a 3d panel method. In *16th International Forum on Aeroelasticity and Structural Dynamics*.
- [17] Parenteau, M., Plante, F., Laurendeau, E., et al. (2017). Unsteady coupling algorithm for lifting-line methods. In *AIAA SCITECH 2017 Forum*. doi:10.2514/6.2017-0951.
- [18] Parenteau, M. and Laurendeau, E. (2020). A general modal frequency-domain vortex lattice method for aeroelastic analyses. *Journal of Fluids and Structures*, 99, 103146. ISSN 0889-9746. doi:10.1016/j.jfluidstructs.2020.103146.
- [19] Bekemeyer, P., Ripepi, M., Heinrich, R., et al. (2019). Nonlinear unsteady reduced-order modeling for gust-load predictions. *AIAA Journal*, 57(5), 1839–1850. doi: 10.2514/1.J057804.

- [20] Katz, J. and Plotkin, A. (2001). *Low-Speed Aerodynamics, Second Edition*. New York: Cambridge University Press.
- [21] European Union Aviation Safety Agency, E. (2021). *CS-25 Large Aeroplanes (Amendment 27)*.
- [22] Wright, J. R. and Cooper, A. J. E. (2014). *Introduction to Aircraft Aeroelasticity and Loads, Second Edition*. West Sussex: Wiley.
- [23] Sears, W. R. (1941). Some aspects of non-stationary airfoil theory and its practical application. *Journal of Aeronautical Sciences*, 8(3), 104–108. doi:/10.2514/8.10655.
- [24] Goland, M. (1945). The flutter of a uniform cantilever wing. *Journal of Applied Mechanics*, 12(4), A197–A208. doi:/10.1115/1.4009489.
- [25] Taha, H. E. and Rezaei, A. S. (2019). *On the Dynamics of Unsteady Lift and Circulation and the Circulatory-Non-circulatory Classification*. doi:10.2514/6.2019-1853.
- [26] Cook, R. G., Palacios, R., and Goulart, P. (2013). Robust gust alleviation and stabilization of very flexible aircraft. *AIAA Journal*, 51(2), 330–340. doi:10.2514/1.J051697.
- [27] Wales, C., Valente, C., Cook, R., et al. (2018). The future of non-linear modelling of aeroelastic gust interaction. In *2018 Applied Aerodynamics Conference*. doi:10.2514/6.2018-3632.

COPYRIGHT STATEMENT

The authors confirm that they, and/or their company or organization, hold copyright on all of the original material included in this paper. The authors also confirm that they have obtained permission, from the copyright holder of any third party material included in this paper, to publish it as part of their paper. The authors confirm that they give permission, or have obtained permission from the copyright holder of this paper, for the publication and distribution of this paper as part of the IFASD-2022 proceedings or as individual off-prints from the proceedings.